Polarized Raman Spectroscopy on Isolated Single-Wall Carbon Nanotubes

G. S. Duesberg,[1,2] I. Loa,[1] M. Burghard,[1] K. Syassen,[1] and S. Roth[1]

[1]*Max-Planck-Institut für Festkörperforschung, Heisenbergstrasse 1, D-70569 Stuttgart, Germany*

[2]*Physics Department, Trinity College Dublin, College Green, Dublin 2, Ireland*

(Received 14 April 2000)

Polarized micro-Raman spectroscopy has been performed on spatially separated single-wall carbon nanotubes (SWNTs) in the form of individual nanotubes or thin ropes of only a few SWNTs. Different from bulk samples, the Raman spectra are composed of well-resolved peaks which allow a direct comparison of experimental data with theoretical calculations. Orientation-dependent measurements reveal maximum intensity of all Raman modes when the nanotubes are aligned parallel to the polarization of the incident laser light. The angular dependences clearly deviate from the selection rules predicted by theoretical studies. These differences are attributed to depolarization effects caused by the strongly anisotropic geometry of the nanotubes and to electronic resonance effects for excitation at 633 nm.

PACS numbers: 78.30.Na

Single-wall carbon nanotubes (SWNTs) are macromolecules which can be metallic, semimetallic, or semiconducting depending on their structure [1]. In view of the numerous potential applications of SWNTs, which include field emission [2], hydrogen storage [3], single electron transistors [4], gas sensors [5], and nanomechanical devices [6], the characterization of their physical properties is an important issue. One of the most promising techniques for this task is Raman spectroscopy [7].

Most Raman studies have been performed on bulk samples varying in purity, morphology, and diameter distribution of the SWNTs. The obtained spectra are a superposition of contributions from different, nonaligned SWNTs, causing rather broad and unresolved peaks. Because of electronic resonance effects the contributions of different tubes to the Raman spectrum vary when recorded with different laser energies [8–12]. The spectra of bulk samples are therefore dominated by contributions from resonantly excited tubes. Thus, in practice the complexity of the spectra impedes an interpretation based on calculations for *individual* SWNTs [12]. Investigations of single nanotubes are desirable to overcome these problems. Individual SWNTs and small ropes were recently studied by surface-enhanced Raman spectroscopy, revealing well-resolved spectra [13]. One study on monodispersed, aligned SWNTs hosted in crystal channels has been presented [14]. The spectra, however, are considerably different from those of conventional SWNT samples synthesized by arc discharge or laser ablation.

In this Letter, we present the first orientation-dependent Raman spectra of spatially separated thin ropes of SWNTs consisting of only a small number of nanotubes. The experiments were performed *without employing surface-enhancement techniques* in order to study the intrinsic Raman selection rules of carbon nanotubes. The orientation dependence of the intensity of all investigated Raman modes shows an unexpected twofold symmetry, where the maximum signal is always observed when the polarization of the incident light is parallel to the nanotube axis. This is ascribed to depolarization effects due to the very anisotropic shape of the nanotubes and to electronic resonance effects which cause a breakdown of selection rules. So far, these effects have not been considered in calculations of SWNT Raman spectra.

The SWNTs were produced by the arc discharge method with Ni/Y catalysts [15]. The raw material was suspended in an aqueous sodium dodecylsulfate solution and purified by chromatography as previously described [16]. The separated SWNTs were adsorbed on polished and surface-treated Suprasil glass substrates with gold electrode markers as described previously [17]. In the areas close to the marker electrodes the SWNTs were characterized with a scanning force microscope [(SFM), Digital Instruments, Nanoscope IIIa] in tapping mode.

Raman spectra were excited with a He/Ne laser (632.8 nm) and recorded using a micro-Raman setup (Renishaw System 2000) which offers the very high optical efficiency necessary to detect the weak signal of individual SWNTs. A 100× microscope objective was used for focusing of the laser beam and collection of the scattered light. The laser spot had a diameter of $\sim 1\ \mu$m at the sample with a power density of $\sim 10^5$ W/cm^2. For the orientation-dependent and polarized measurements a half-wave retardation plate was inserted before the microscope objective to rotate the polarization of the incident laser beam and of the scattered light (see inset in Fig. 3). This twofold rotation of the polarization is equivalent to an effective rotation of the nanotube in the horizontal plane. All Raman spectra were taken in backscattering configuration, with the incident and scattered light propagating perpendicular to the nanotube axis.

The SFM image of SWNTs on a glass substrate (Fig. 1) shows that the marked objects No. 1, No. 2, and No. 3 are well separated and each is $\sim 1.5\ \mu$m long. The height of object No. 1 of ~ 1.5 nm corresponds to that of an individual SWNT. The limited lateral resolution of SFM generally does not allow one to distinguish between an individual SWNT and a raft of a few SWNTs. Objects No. 2

 0031-9007/00/85(25)/5436(4)$15.00

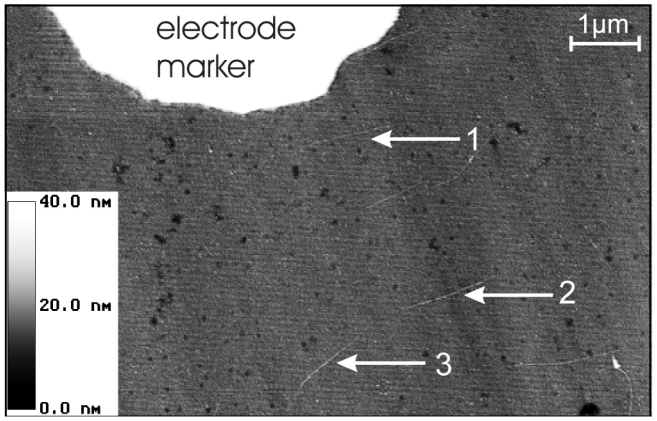

FIG. 1. SFM image of well-separated individual SWNTs and small bundles of SWNTs adsorbed on a glass substrate. The end of a gold electrode used as a marker can be seen at the upper left. The height of object No. 1 corresponds to that of an individual SWNT, while No. 2 and No. 3 are small ropes of SWNTs.

and No. 3 are small ropes with a height of ~5 nm. The electrode end (top left of Fig. 1) was used as a landmark to position the laser spot on each of the marked objects.

In Fig. 2(a) the spectrum of object No. 1 is presented together with that of the substrate as a reference. The G line of graphite at 1580 cm^{-1} (E_{2g} symmetry) is split into several modes when a graphene sheet is bent to a cylinder. In Fig. 2(a) the G band consists of a broad and intense peak G_1 at 1550 cm^{-1}, commonly attributed to resonantly excited metallic SWNTs [10], and a narrow feature G_2 at 1580 cm^{-1}. This band shape and the pronounced D line at 1318 cm^{-1} have been observed for all objects investigated in our experiment. In Fig. 2(b) the low-frequency regions of the spectra of objects No. 1–3 are highlighted. All three objects show a single, nearly symmetric radial breathing mode (RBM), where the carbon atoms undergo a uniform radial displacement perpendicular to the tube axis.

Single thin and straight objects were selected for the orientation-dependent measurements. Figure 3 displays Raman spectra with different angles α_i between the polarization (electric field) of the incident laser light and the nanotube axis. The spectra were recorded with parallel polarizations of the incoming and scattered light ("VV configuration"). All modes show maximum intensity when the polarization of the incident radiation is parallel to the nanotube axis ($\alpha_i = 0°$ and $\alpha_i = 180°$), while near 90° no signal could be detected. This orientation dependence was fully reproducible for several distinct objects.

It is noteworthy that the relative intensities of the RBM and the G line were found to vary significantly for different objects with ratios $I_{\mathrm{RBM}}/I_G = 0.1–4$. This effect is not

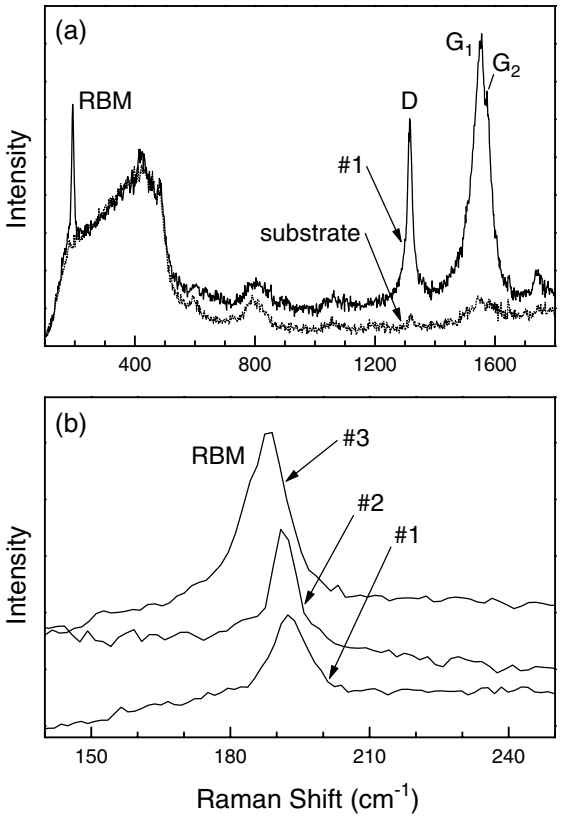

FIG. 2. (a) Raman spectrum of object No. 1 (see Fig. 1) with the polarization of the incident laser beam parallel to the axis of the SWNT. The dotted line is the spectrum of the bare substrate. The symmetric D line is centered at 1318 cm^{-1} and has been observed on all objects. (b) Raman spectra of objects Nos. 1–3 in the low-frequency region.

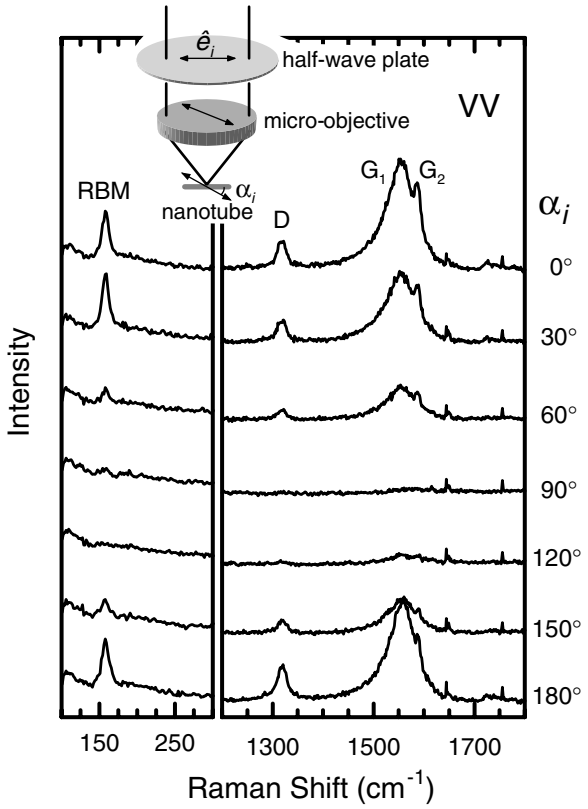

FIG. 3. Raman spectra of a thin SWNT rope in the VV configuration for various angles α_i between the rope axis and the polarization of the incident laser beam, as depicted in the inset. For $\alpha_i = 0°$ and 180° the polarization of the incident radiation is parallel to the axis of the SWNTs determined from SFM images with an accuracy of ±10°.

related to possibly different orientations α_i of the various objects, as all modes exhibit the same angular dependence.

The complete angular dependences of the intensities $I(\alpha_i)$ of the D line and the components G_1 and G_2 of the G line are shown in Fig. 4(a) for the VV scattering configuration. Figure 4(b) displays the orientation dependence of the RBM signal for both parallel VV and crossed VH polarizations of incident and scattered light. The same behavior was also observed for the cross-polarized Raman spectra of the higher-energy modes. Thus, the intensities of all Raman modes in both the parallel- and the cross-polarized configuration show the same angular dependence which can be described by $I(\alpha_i) \propto \cos^2(\alpha_i)$ (solid lines). This means that the Raman signal is maximum with the incident polarization parallel to the tube axis and zero when perpendicular. It further implies that the two cross-polarized scattering configurations VH ($\alpha_i = 0°$) and HV ($\alpha_i = 90°$) are not equivalent.

The RBM frequency was calculated to scale (almost independently of the helicity of the tube) with the inverse diameter d of a given SWNT [18–21]. The relation $d(\text{nm}) = 224/\omega(\text{cm}^{-1})$ was proposed by Bandow *et al.* [22], where ω is the Raman frequency of the RBM. This provides a Raman-spectroscopy-based measure for the diameter of individual SWNTs which so far could be determined only by scanning tunneling microscopy or transmission electron microscopy.

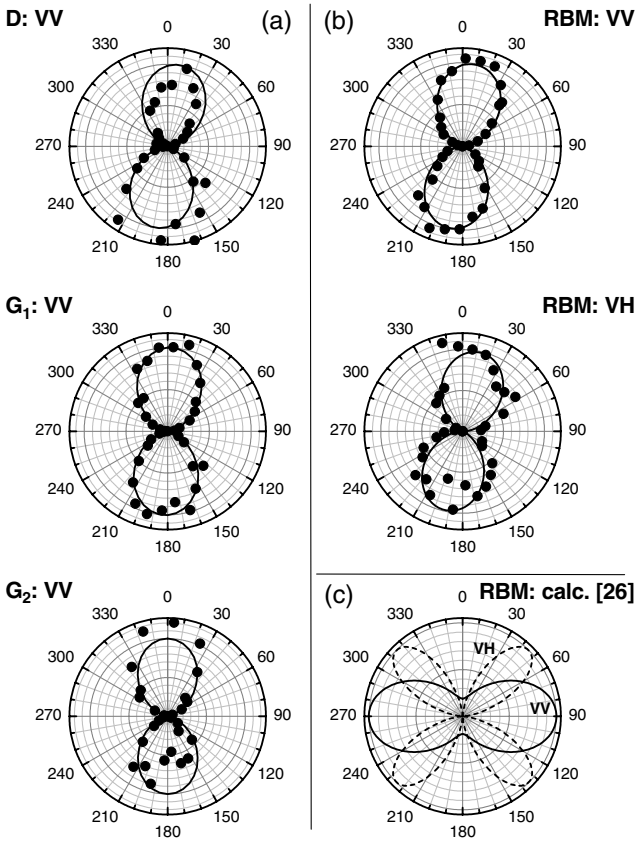

FIG. 4. Polar diagrams showing the Raman mode intensities I of SWNTs as a function of the angle α_i between the polarization of the incident light and the nanotube axis. $I(\alpha_i)$ for (a) the components G_1 and G_2 of the G line and for the D line in the VV scattering configuration and (b) the RBM in the VV and VH configurations. The twofold symmetry of the modes, which can be modeled by $I(\alpha_i) \propto \cos^2(\alpha_i)$, has been observed on all investigated objects. (c) Calculated $I(\alpha_i)$ for the RBM of a (10, 10) tube under nonresonant conditions after data of Ref. [26].

Interestingly, most of the thin ropes studied here exhibit symmetric, sharp RBMs, suggesting that they are composed of SWNTs very similar in diameter. Recent experimental [23] and theoretical [24,25] results show that the RBM frequency is up-shifted by 5%–10% for tubes packed into bundles. Therefore, the absolute diameter cannot be determined at high accuracy from the frequency of the RBM, as long as the effect of the surrounding environment is not precisely known. It is, however, possible to distinguish tubes of different diameter by their RBM positions at high precision. For example, a change in diameter of only 0.01 nm relates to a shift of the RBM frequency by more than 1 cm^{-1}, which is determined easily.

Based on lattice-dynamical calculations [8,24], it is generally accepted that the components of the SWNT G mode have E_{2g}, A_{1g}, E_{1g} (zigzag or armchair SWNTs) or E_2, A_1, E_1 symmetry (chiral SWNTs) and that the RBM has A_{1g} (A_1) symmetry. Saito *et al.* have calculated the angular dependences for all modes under nonresonant conditions for a (10, 10) armchair tube [26] as reproduced in Fig. 4(c) for the RBM in VV (solid line) and VH (dashed line) scattering configurations. The measured angular dependences presented here do not reflect the different symmetries and they are not compatible with the predictions for any of the symmetries A_{1g}, E_{1g}, or E_{2g}. All modes exhibit the same twofold symmetry in the VV and VH configurations with the highest intensity occurring when the incident radiation is polarized parallel to the tube axis. $A_{1(g)}$ symmetry of the RBM implies zero Raman scattering intensity for the cross-polarized VH configuration when the incident radiation is polarized parallel ($\alpha_i = 0°$) or perpendicular ($\alpha_i = 90°$) to the tube axis. The maximum signal should occur at $\alpha_i = 45°$. In contrast to this prediction, we experimentally observe the strongest Raman signal in the VH configuration for $\alpha_i = 0°$. These discrepancies may be related to two effects not taken into account so far in the theory: (i) depolarization due to the very anisotropic shape of the tubes and (ii) electronic resonance effects.

SWNTs with a typical length-to-diameter ratio on the order of 1000 are extremely anisotropic. This leads to significantly differing polarizabilities for external fields applied parallel and perpendicular to the tube axis. Ajiki and Ando [27] have calculated the optical conductivity of carbon nanotubes taking into account this geometrical depolarization effect. According to their calculation, the absorption of light polarized parallel to the tube axis is up to $\sim$20 times larger than for perpendicularly polarized light. This leads to a strongly reduced Raman signal when the polarization of the incident radiation is perpendicular to the nanotube axis, as the absorption of a laser photon is one

step in the Raman-scattering process. Experimentally, such depolarization effects have, for instance, been observed for semiconducting and metallic nanowires confined in the channels of asbestos fibers [28,29]. A strongly anisotropic optical absorption was observed and could be explained by the depolarization effect. Furthermore, the Raman spectra of the nanowires were also most intense when the incident polarization was chosen parallel to their axis. A similar polarization effect was also observed in a recent Raman study of aligned and bundled multiwall nanotubes by Rao *et al.* [30].

The breakdown of Raman selection rules is a well-known effect for *resonant* Raman scattering [31]. The broad peak near 1550 cm^{-1} in nanotube spectra excited near 1.9 eV (650 nm) has been associated with resonantly excited metallic tubes [10]. The unexpected observation of a strong RBM signal in the cross-polarized case (with $\alpha_i = 0°$) and excitation at 633 nm may thus be related to resonance effects. Further experiments with different excitation wavelengths should be performed to clarify this point.

The mode at 1318 cm^{-1} is known as the disordered carbon line (D line) and in the case of nanotubes it is generally attributed to the presence of amorphous carbon in bulk samples. The separated and purified SWNTs used in this study do not contain significant amounts of amorphous carbon which could account for the intense D mode. Together with the measured orientation dependence of this line it clearly shows that the mode at 1318 cm^{-1} is an inherent feature of SWNTs and may be related to symmetry lowering effects, e.g., defects, bending of the nanotubes, or finite-size effects [7].

In conclusion, polarization-dependent Raman spectra of oriented SWNTs have been presented. For all modes and scattering configurations the Raman signal is strongest when the polarization of the incident radiation is parallel to the nanotube axis and vanishes when perpendicular. The breakdown of the predicted selection rules is attributed to depolarization, caused by the anisotropic shape of the nanotubes, and to resonance effects. It is shown that the D line is an intrinsic part of the Raman spectrum of SWNTs. Although single-molecule Raman spectroscopy has been proposed for molecules like DNA sequences, spectra could up to now be obtained only using surface enhancement methods [32,33], which generally strongly affect Raman selection rules. By contrast our study shows that a Raman investigation of individual macromolecules of specified location and orientation is now possible without surface enhancement techniques. In addition, this method is not invasive and is performed under ambient conditions and therefore opens the possibility of, for example, characterizing individual SWNTs incorporated into devices.

We gratefully thank H. J. Byrne (Dublin Institute of Technology), W. Blau (Trinity College Dublin), J. Muster (MPI für Festkörperforschung, Stuttgart), and N. Nicoloso (University of Stuttgart) for helpful discussions. This work has been supported by the EU TMR network NAMITECH, ERBFMRX-CT96-0067 (DG-MIHT).

[1] M. Dresselhaus, G. Dresselhaus, and P. Eklund, *Science of Fullerenes and Carbon Nanotubes* (Academic Press, New York, 1996).
[2] S. S. Fan *et al.,* Science **283**, 512 (1999).
[3] C. Liu *et al.,* Science **286**, 1127 (1999).
[4] S. J. Tans, A. R. M. Verschueren, and C. Dekker, Nature (London) **393**, 49 (1998).
[5] J. Kong *et al.,* Science **287**, 622 (2000).
[6] P. Kim and C. M. Lieber, Science **286**, 2148 (1999).
[7] R. Saito, G. Dresselhaus, and M. Dresselhaus, *Physical Properties of Carbon Nanotubes* (Imperial College Press, London, 1998).
[8] A. M. Rao *et al.,* Science **275**, 187 (1997).
[9] H. Kataura *et al.,* Synth. Met. **103**, 2555 (1999).
[10] M. A. Pimenta *et al.,* J. Mater. Res. **13**, 2396 (1998).
[11] A. Kasuya *et al.,* Phys. Rev. B **57**, 4999 (1998).
[12] M. Milnera, J. Kürti, M. Hulman, and H. Kuzmany, Phys. Rev. Lett. **84**, 1324 (2000).
[13] G. S. Duesberg *et al.,* Chem. Phys. Lett. **310**, 8 (1999).
[14] H. D. Sun, Z. K. Tang, J. Chen, and G. Li, Solid State Commun. **109**, 365 (1999).
[15] C. Journet *et al.,* Nature (London) **388**, 756 (1997).
[16] G. S. Duesberg *et al.,* Appl. Phys. A **67**, 117 (1998).
[17] M. Burghard *et al.,* Adv. Mater. **10**, 584 (1998).
[18] E. Richter and K. R. Subbaswamy, Phys. Rev. Lett. **79**, 2738 (1997).
[19] J. Kürti, G. Kresse, and H. Kuzmany, Phys. Rev. B **58**, R8869 (1998).
[20] D. Sánchez-Portal *et al.,* Phys. Rev. B **59**, 12 678 (1999).
[21] V. N. Popov, V. E. Van Doren, and M. Balkanski, Phys. Rev. B **59**, 8355 (1999).
[22] S. Bandow *et al.,* Phys. Rev. Lett. **80**, 3779 (1998).
[23] U. D. Venkateswaran *et al.,* Phys. Rev. B **59**, 10 928 (1999).
[24] D. Kahn and J. P. Lu, Phys. Rev. B **60**, 6535 (1999).
[25] L. Henrard, E. Hernández, P. Bernier, and A. Rubio, Phys. Rev. B **60**, R8521 (1999).
[26] R. Saito *et al.,* Phys. Rev. B **57**, 4145 (1998).
[27] H. Ajiki and T. Ando, Physica (Amsterdam) **201B**, 349 (1994).
[28] V. V. Poborchii, Jpn. J. Appl. Phys. **34**, Suppl. 34-1, 271 (1995).
[29] V. V. Poborchii *et al.,* J. Phys. Condens. Matter **9**, 5687 (1997).
[30] A. M. Rao *et al.,* Phys. Rev. Lett. **84**, 1820 (2000).
[31] M. Cardona, in *Light Scattering in Solids, II, Basic Concepts and Instrumentation,* Topics in Applied Physics, edited by M. Cardona and G. Güntherrodt (Springer-Verlag, Berlin, Heidelberg, New York, 1982), Vol. 50, p. 19ff.
[32] K. Kneipp *et al.,* Chem. Rev. **99**, 2957 (1999).
[33] H. X. Xu, E. J. Bjerneld, M. Käll, and L. Börjesson, Phys. Rev. Lett. **83**, 4357 (1999).